Effect of the Incorporation a Commercial Ricinus communis Extract on the Morphology and Properties of Poly (lactic acid) Electrospun Mats

Efecto de la incorporación de un extracto comercial de Ricinus communis en la morfología y las propiedades de las matrices electro-hiladas de poliácido láctico

Javier M. Anaya-Mancipe [1], José A. Anaya-Mancipe [2], Marceli N. da Conceição [3], and Rossana M. S. M. Thiré [4]

ABSTRACT

Chronic skin wounds represent a major challenge in healthcare, necessitating the development of advanced biomaterials capable of promoting healing while maintaining structural integrity. In this study, poly(lactic acid) (PLA) nanofibrous mats were produced via electrospinning and loaded with a commercial extract of Ricinus communis (castor seed oil) as a potential dressing material. The process was performed in two phases: first, the optimal electrospinning parameters (voltage and flow rate) were selected by means of an analysis of variance (ANOVA); subsequently, the castor oil extract was incorporated into the PLA solution. Morphological and chemical analyses were carried out using scanning electron microscopy (SEM) and Fourier-transform infrared spectroscopy (FTIR). The wettability and absorption capacity were evaluated through contact angle measurements and swelling tests. The incorporation of castor oil increased swelling by 60% without affecting the contact angle (132°), indicating reductions in hydrophobicity without compromising surface characteristics. Additionally, the presence of excipients in the commercial extract affected the thermal behavior and crystallinity of the PLA. These findings highlight the potential of electrospun PLA mats containing Ricinus communis extract as functional wound dressing materials, combining biocompatibility, structural performance, and tunable physical properties for chronic wound management.

Keywords: nanofibers, phytopharmaceuticals, tissue engineering, drug delivery, biomaterials

RESUMEN

Las heridas cutáneas crónicas representan un desafío importante en el ámbito de la salud, lo que requiere el desarrollo de biomateriales avanzados capaces de promover la cicatrización a la vez que se mantiene la integridad estructural. En este estudio se produjeron mantas fibrosas de poli(ácido láctico) (PLA) mediante electrohilado y se incorporó un extracto comercial de Ricinus communis (aceite de ricino) como posible material para apósitos. El proceso se realizó en dos fases: primero, se seleccionaron los parámetros óptimos de electrohilado (voltaje y caudal) mediante un análisis de varianza (ANOVA); posteriormente, se incorporó el extracto al polímero. Se realizaron análisis morfológicos y químicos mediante microscopía electrónica de barrido (SEM) y espectroscopía infrarroja por transformada de Fourier (FTIR). La mojabilidad y la capacidad de absorción se evaluaron mediante ensayos de hinchamiento y mediciones del ángulo de contacto. La incorporación del extracto incrementó el grado de hinchamiento en un 60 % sin alterar el ángulo de contacto (132°), indicando una menor hidrofobicidad sin comprometer la superficie. Además, los excipientes del extracto afectaron el comportamiento térmico y la cristalinidad del PLA. Estos resultados destacan el potencial de las mantas electrohiladas de PLA con extracto de Ricinus communis como apósitos funcionales, combinando biocompatibilidad, desempeño estructural y propiedades físicas ajustables para el manejo de heridas crónicas.

Palabras clave: Nanofibras, Fitofármacos, Ingeniería de tejidos, Liberación de fármacos, Biomateriales

[1] Chemical engineer – Universidad Industrial de Santander (UIS), Colombia. DSc Engenharia Metalúrgica e de Materiais (PEMM/COPPE), Universidade Federal do Rio de Janeiro – UFRJ, Brazil. Email: javier.anaya@metalmat.ufrj.br

[2] Petroleum engineer – Universidad Industrial de Santander (UIS), Colombia. Master student in Metallurgical and Materials Engineering (PEMM/COPPE), Universidade Federal do Rio de Janeiro – UFRJ, Email: anayamancipe_04@hotmail.com

[3] Materials engineer – Universidade do Estado de Rio de Janeiro (UERJ), Brazil. DSc Engenharia Metalúrgica e de Materiais (PEMM/COPPE), Universidade Federal do Rio de Janeiro – UFRJ, Brazil. Email: marceli@metalmat.ufrj.br

[4] Chemical engineer – Universidade Federal do Rio de Janeiro (UFRJ), Brazil. DSc Engenharia Metalúrgica e de Materiais (PEMM/COPPE/UFRJ), Brazil. Associate professor, DEMM-PEMM/COPPE, Universidade Federal do Rio de Janeiro (UFRJ), Brazil. Email: rossana@metalmat.ufrj.br

Introduction

The skin is the largest organ of the human body, acting as a protective barrier and blood reservoir [1]. However, its external exposure makes it vulnerable to environmental factors such as heat, humidity, and friction, which can compromise structural integrity and lead to wound formation [2]. Treating chronic wounds remains challenging, as it requires solutions that combine efficacy, safety, and accessibility [3].

In recent years, the use of advanced biomaterials with incorporated bioactive compounds has emerged as a promising approach to accelerate wound healing [4], [5]. Electrospinning, widely employed for producing nanostructured mats, enables the incorporation of active molecules into polymeric matrices, generating fibrous scaffolds with high surface area and tunable porosity that promote tissue regeneration and controlled release [6], [7], [8].

Among the bioactive compounds, castor oil (*Ricinus communis*) has attracted attention due to its pharmacological properties. Rich in ricinoleic acid (~90%) and other fatty acids, castor oil exhibits anti-inflammatory, antimicrobial, and regenerative effects [9]. *In vitro* studies have shown that it stimulates cell proliferation and collagen synthesis, accelerating healing [10], while preclinical trials have confirmed its efficacy in reducing inflammation and tissue regeneration time. However, exposure to environmental conditions may trigger the oxidation of secondary metabolites, compromising stability and efficacy [11].

Several studies have reported the incorporation of castor oil into polymeric systems, mainly as a plasticizer or functional modifier. [12] synthesized branched PLA with a castor oil core, demonstrating a reduced glass transition temperature (Tg) and an enhanced chain mobility. [13] incorporated natural and modified castor oil into PLA during melt processing, confirming changes in crystallinity, thermal stability, and mechanical performance. [14] developed electrospun polyurethane/castor oil scaffolds for cardiovascular applications, highlighting the potential of castor oil to improve flexibility and biocompatibility in fibrous systems. These works confirm the versatility of castor oil as a functional additive.

Beyond castor oil, other natural extracts have also been incorporated into PLA matrices in order to modulate physicochemical behavior. For instance, [15] prepared PLA/babassu oil membranes with improved hydrophilicity and swelling. [16] incorporated peppermint essential oil into PLA nanofibers, modifying crystallinity and thermal transitions. [17] studied PLA/castor oil blends via melt processing, reporting changes in degradation kinetics. Similar effects have been reported for PLA-based fibers containing bacitracin and *Zataria multiflora* extract [18], silver nanoparticles [19], and other phytocompounds [20], [21], confirming that natural additives strongly influence fiber morphology, viscosity, and polymer crystallinity. Despite these advances, no study has systematically evaluated the incorporation of a commercial pharmaceutical formulation of castor oil into electrospun PLA fibers. Products such as Linitul, which combine castor oil with excipients (*e.g.*, Peru balsam, petroleum jelly, paraffin, dimethicone) [22], may significantly affect spinnability, morphology, thermal stability, and absorption properties.

This study addressed this gap by investigating the morphological, chemical, thermal, and functional properties of PLA mats with a castor oil-based extract (COE) intended for wound dressing applications.

We hypothesized that incorporating a COE into electrospun PLA mats will act as a functional plasticizer, enhancing moisture absorption and flexibility while preserving fiber integrity. To test this, PLA mats were characterized via scanning electron microscopy (SEM, morphology), Fourier transform infrared spectroscopy (FTIR, chemical interactions), thermalgravimetric analysis (TGA), and differential scanning calorimetry (DSC, thermal behavior). Dynamic mechanical analysis (DMA) was performed to evaluated the mechanical response and infer the miscibility between PLA and COE. Wettability (contact angle) and exudate absorption capacity (swelling degree) were also assessed. The following sections describe the experimental procedures, present and discuss the results, and conclude with the main findings of this study.

Materials and methods

Materials

Poly(lactic acid) pellets (Mn: 71 931 g/mol; Mw: 122 080 g/mol, PDI: 1.72) (Ingeo Bio-polymer 2003D, NatureWorks LLC) were purchased from BASF. Analytical grade chloroform (Chl) was purchased from Exôdo Cientifica SA in Rio de Janeiro, and dimethylformamide (DMF) was obtained from Sigma-Aldrich in São Paulo, Brazil. The *Ricinus communis* extracts (castor oil – COE) were purchased as a commercial cream (Linitul) from Madrid, Spain.

Solution preparations

Initially, we conducted an electrospinning parameter study. To this effect, three different solutions with 15, 17.5, and 20 wt.% PLA concentrations were prepared using a Chl/DMF solvent system with a volumetric ratio of 7:3, under magnetic stirring for 4 h at room temperature [14]. Afterwards, 5 ml of the PLA solution were prepared (15 wt.%), incorporating three different concentrations in 0, 10, and 20 wt.% of the COE as a function of the polymer mass ratio, denoted as PLA00, PLA10, and PLA20. The solutions were subjected to magnetic stirring for 1 h at room temperature.

Electrospinning process

To produce the PLA/COE mats, a horizontal electrospinning system was employed, comprising a high-voltage source (PS/FC 60p02.0-1), a KDS 100 series syringe pump for injection, and an aluminum collection plate grounded with a wire. Each solution (5 ml) was loaded into a plastic syringe fitted with a 24-gauge metal needle. Electrospun PLA fibers were produced using a fixed needle-to-collector distance of 17 cm, while the applied voltage (12.5, 15, and 17 kV) and the flow rate (0.5, 0.75, and 1.0 mL/h) were varied.

Characterization

Viscosimeter. Rheological measurements of the PLA00, PLA10, and PLA20 solutions were performed using a ViscoQC-100 rotational viscosimeter (Anton Paar Trading Co., Shanghai) and a CC18 spindle. The shear rate was varied (1-10 rpm) at room temperature.

Surface tension. The surface tension of the three PLA solutions with and without COE was determined using the drop methods described by [23]. To this effect, 50 drops of each solution were weighed in an analytical balance (AY220, Shimadzu Brazil LTDA, São Paulo, Brazil). The surface tension value (γ_w) was calculated using the water tension (0.072 N/m), the weight of the PLA solution (50 drops), and the weight of water, as showin in Eq. (1).

$$\gamma_x = \frac{\gamma_w * M_x}{M_d} \tag{1}$$

Scanning electron microscopy (SEM). The PLA fibers' morphology with and without the extract was evaluated by SEM. To this effect, we used a Tescan VEGA (Czech Republic). The samples were coated with carbon for 120 s before the SEM analysis. The fiber diameters were measured using SEM images in the SizerMeter.1 software, with n = 50 per sample.

Chemical composition (FTIR-ATR). The mats' composition and the chemical interaction between the polymer and the extract (COE) were evaluated in a Fourier transform infrared (FTIR) spectrophotometer (model 6000, Thermo Scientific) with an attenuated total reflectance accessory (ATR). The analysis was performed in the 4000-650cm⁻¹ region, with 128 scans and a resolution of 4cm⁻¹.

Thermal behavior (TGA-DSC). The thermal stability and weight loss of the electrospun mats and the pure dry extract were evaluated by means of a thermogravimetry analysis, using Shimadzu TGA-50 with a heating range of 25 to 700 °C and a heating rate of 10 °C/min under a N_2 atmosphere.

The thermal transition of the PLA/COE composite was performed through differential scanning calorimetry (DSC), using Shimadzu equipment. Approximately 10 mg of each sample were used in this analysis, conducted at rate of 10 °C/min under a N_2 atmosphere with a flow rate of 50 mL/min. The samples were analyzed in two heating and one cooling cycle. The first heating cycle went from 20 to 180 °C, followed by one cooling cycle (180 to 0 °C). The second heating cycle took place at 180 °C. The analysis was conducted under a nitrogen gas flow. Crystallinity (Xc) was calculated using Eq. (2).

$$X_c = \frac{\Delta H_f}{\Delta H^{\circ}_f} \tag{2}$$

where ΔH_f is the melting enthalpy of the endothermic peak of the DSC thermogram (second heating cycle), and ΔH°_f =106 j/g is the theoretical melting enthalpy for a 100% crystalline PLA sample [24].

Mechanical behavior. Tensile tests were performed on the PLA/COE electrospun mats using a dynamic mechanical analysis (DMA, TA Instrument Q800, USA) in controlled force mode. A pre-load of 0.05 N was applied, and the specimens were stretched at a rate of 0.1 N/min until failure at room temperature ($\sim 25°C$). Three tests were performed for each sample (n = 3), with dimensions of 30 x 5 mm and a thickness of about 1 mm [25].

Wettability. A contact angle analysis was performed in order to evaluate the wettability of the mats with the variation in the COE mass ratio (PLA00, PLA10, and PLA20). To this effect, we used a Ramé-Hart NRL A 100-00 goniometer. A drop of distilled water (4 µL) was deposited on the surface of each mat at room temperature. The contact angles were measured in triplicate.

Swelling. The swelling capacity of the PLA00, PLA10, and PLA20 electrospun mats was tested in two phosphate-buffered saline solutions (PBS, pH=7.4 and 4.0). The degree of swelling (SD) of the samples was calculated in triplicate (n=3) using Eq. (3).

$$SD_c (\%) = 100x \frac{W_s - W_D}{W_D} \tag{3}$$

where W_s is the weight of the swollen sample at a given time, and W_D is the initial mass of the mats (dry weight) [16].

Statistical analysis. All data were expressed as the mean ± standard deviation of at least three samples. A one-way analysis of variance (ANOVA) was conducted to determine the statistical significance of the data. This was done using Origin 9.1. A value of $p < 0.05$ was considered to be statistically significant.

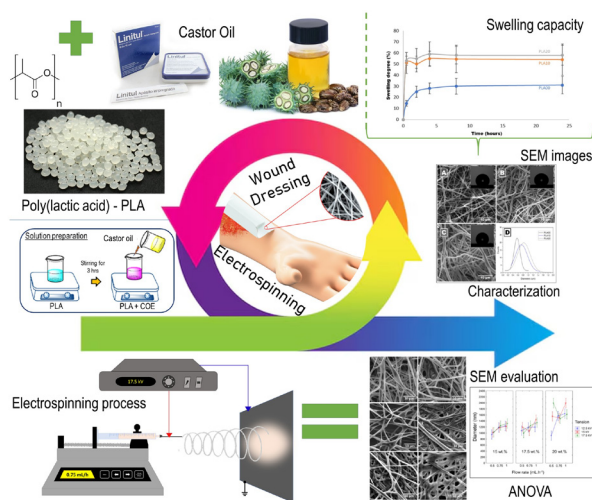The production and characterization of the wound dressing is depicted in Fig. 1.

Figure 1. Scheme of the experimental procedure used in this study, including electrospinning optimization, castor oil extract incorporation, and physicochemical characterizations
Source: Authors

Results and discussion

Before discussing the experimental results, it is important to emphasize that, unlike most studies that employ pure castor oil, this work incorporates a commercially available and clinically used formulation (Linitul). This product consists not only of castor oil but also includes Peru balsam and a complex mixture of excipients such as petroleum jelly, beeswax, paraffin, and dimethicone [22]. These components can significantly influence both the properties of the solution and the final characteristics of the electrospun mats, *i.e.*, its morphology, crystallinity, and fluid absorption. Therefore, the results presented herein offer a more realistic and application-oriented understanding of the use of phytopharmaceutical formulations in electrospun wound dressings.

Spinnability study and PLA solutions

The initial focus of this study corresponded to variations in electrospinning parameters such as flow rate, voltage, polymer concentration, and their interaction. Accordingly, three solutions with 15, 17.5, and 20 wt.% PLA were prepared, using a binary solvent system of chloroform and dimethylformamide (Chl/DMD, 7:3). The SEM micrographs of these samples, which highlight the morphology of the produced fibers, are presented in Figs. 2, 3, and 4 for the solutions with 15, 17.5, and 20 wt.%, respectively. These images reveal that the three concentrations lead to intra- and intermolecular interactions of the polymer, as well as to a sufficient entanglement of the polymer chains to support the plastic deformation experienced during the electrospinning process, thus producing continuous fibers free of defects. The fibers obtained in this study had average diameters ranging from 0.9 to 2 μm, which is characteristic of this type of polymer (PLA) when processed via electrospinning [17], [18].
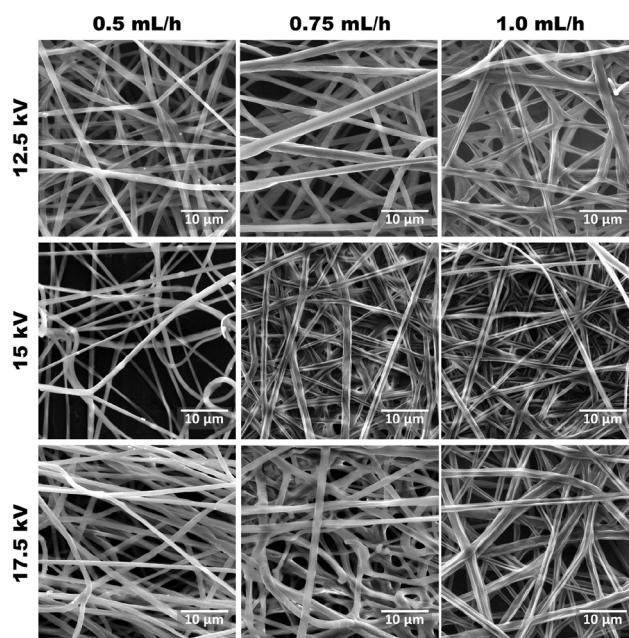

Figure 2. SEM images of electrospun PLA fibers obtained from a 15 wt.% PLA solution. Variations: flow rate and voltage (17 cm needle-to-tip distance).
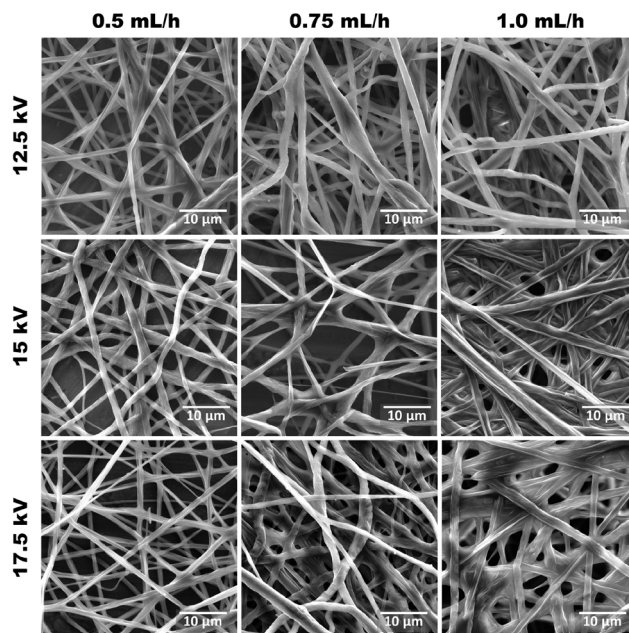**Source:** Authors

Figure 3. SEM images of electrospun PLA fibers obtained from a 17.5 wt.% PLA solution. Variations: flow rate and voltage (17 cm needle-to-tip distance).
Source: Authors

Our study demonstrates that increasing the flow rate yields larger average fiber diameters for less concentrated solutions. This is consistent with the reported literature, which attributes this behavior to the fact that a higher flow rate offers a greater availability of polymer mass as the needle tip, leading not only to larger average fiber diameters,

but also to a greater diameter dispersion [27]. However, for higher-concentration solutions, the diameters did not follow this trend, which may be associated with instabilities in the Taylor cone and increased difficulties in elongating the polymer solution, probably due to the high surface tension. As observed in Figs. 2, 3, and 4, with samples produced at a flow rate of 1.0 mL/h, the fibers from less concentrated solutions exhibit larger diameters. Conversely, those produced from the 20 wt.% PLA solution display ribbon-like morphologies (Figure 4), particularly in SEM images obtained at 15 kV and at flow rates of 0.5 and 1.0 mL/h. This behavior is likely due to the elevated viscosities, which result in thicker fibers that do not completely evaporate their internal solvent. Consequently, upon contacting the collector plate, these fibers collapse into a planar shape, creating the observed morphology [28].
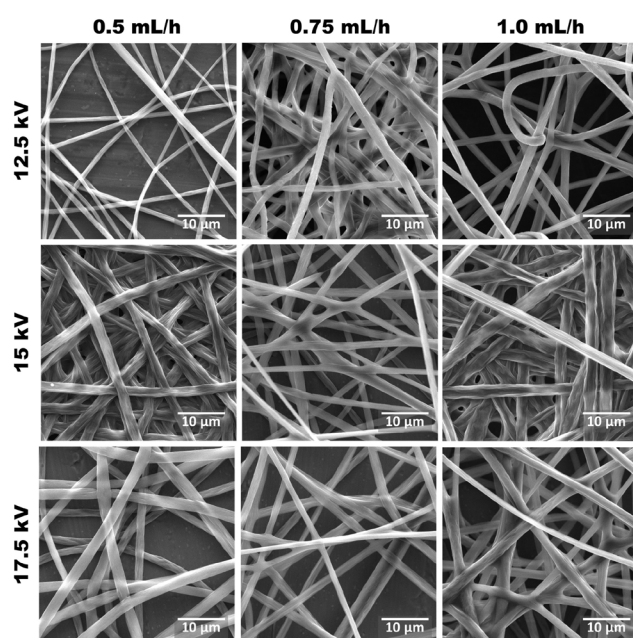

Figure 4. SEM images of electrospun PLA fibers obtained from a 20 wt.% PLA solution. Variations: flow rate and voltage (17 cm needle-to-tip distance).
Source: Authors

These observations corroborate literature reports indicating that high viscosities in polymer solutions significantly increase the surface tension, disrupting the formation of the Taylor cone and leading to the development of dual jets with varying diameters. This, in turn, results in fibers with inconsistent diameters. Additionally, the increased mass and speed of these fibers, coupled with an inadequate solvent evaporation, causes larger fibers to collapse due to the residual solvent. This effect is evident in Figs 3 and 4.

On the other hand, Fig. 5 summarizes the interactions between the studied variables and their influence on the diameter of the produced fibers.

As shown in Fig. 5, the flow rate and voltage variables had a greater impact on the lowest concentration (15 wt.%). This can be attributed to the fact that the polymer mass available for fiber formation is more susceptible to instabilities in the formation of the Taylor cone. This was more pronounced when higher flow rates are used, which resulted in fibers with larger diameters (Fig. 5, left). This behavior was not observed in the fibers produced from more concentrated solutions, as this variable is related to viscosity and surface tension, exhibiting greater difficulties in deforming the polymer solution droplet to produce fibers. This leads to greater variability in fiber diameters, as well as to the collapse and fusion of some fibers, which can be attributed to insufficient solvent evaporation [21].
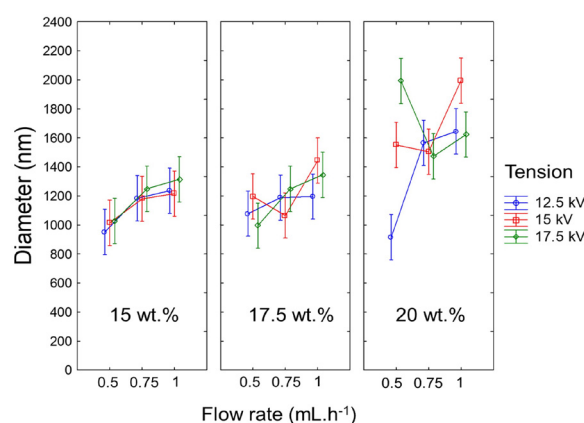

Figure 5. Diagram showing the relationship between fiber diameter and the studied variables
Source: Authors

Based on this information, the polymer solution that yielded the best results in terms of morphology and processing was that with 15 wt.% PLA (Fig. 5). This is why it was selected for the remainder of this study, incorporating its active principle and using electrospinning parameters such as a flow rate of 0.75 ml/h and a voltage of 12.5 kV. The subsequent sections will present the studies carried out on PLA solutions with two COE concentrations, examining how this extract affects the properties of the polymer, as well as its processing via electrospinning.

Evaluating the properties of the PLA/extract solutions

Once the optimal spinning parameters related to the morphology and productive efficiency of the PLA (15 wt.%) used in this study had been established, we incorporated the proposed active ingredient at two concentrations. The results were compared against those obtained with fibers made from pure PLA. This prompted a comparative study and the characterization of neat PLA and its blends with the commercial COE. The literature reports that the active ingredients of Linitul are Peru balsam and castor oil. Each gram of this ointment contains a soluble fraction of 20 mg of Peru balsam and 150 mg of castor oil. The other components

(excipients) are filtered petroleum jelly, liquid petroleum jelly, dimethicone, beeswax, and solid paraffin [22].

Initially, the study was conducted on solutions with and without natural extracts, aiming to understand the molecular interactions between the polymer macromolecules in solution and the extract used in this work (COE). These interactions are crucial in electrospinning, as they influence the efficient formation of fibers. Fig. 6 shows the viscosities and surface tensions of the PLA solutions with and without COE.
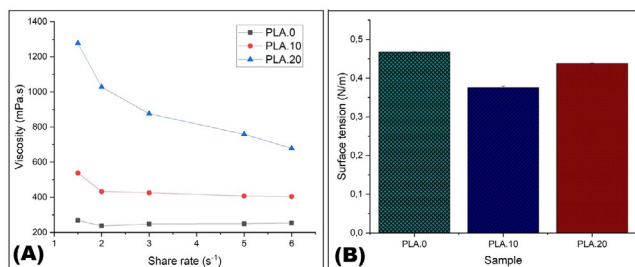

Figure 6. Characterization of PLA solutions under varying extract concentrations: a) viscosity, b) surface tension
Source: Authors

Fig. 6a depicts the variations in viscosity and surface tension observed in the PLA solutions (15 wt. %) with and without two different concentrations of COE. In the electrospinning process, one of the most influential factors in producing defect-free fibers is the concentration of the solution. This is because the polymer macromolecules must exhibit significant intermolecular interactions in order to ensure an efficient entanglement. Such entanglement is crucial, as it allows the polymer to undergo plastic deformation under the repulsive electrostatic forces present during the spinning process.

Fig. 6a illustrates the relationship between viscosity and shear rate. It can be observed that the PLA00 solution follows Newton's law, with the viscosity remaining stable (249.8 ± 10.1 mPa.s) across all shear rates studied. When 10 wt. % COE is added, there is an increase of about 50% increase in viscosity with respect to the neat PLA solution. This behavior can be primarily attributed to the interactions between the various components of the extract and the polymer in the solution. The COE contains excipients such as resins and petroleum jelly, which may act as plasticizers due to their relatively low solubility in the solvents used, especially dimethylformamide (DMF), which is more polar than chloroform. This effect is further corroborated when the concentration of the extract is increased to 20 wt. %, as the solution's behavior changes significantly, becoming a non-Newtonian fluid (Fig. 6a). The viscosity decreases with an increasing shear rate, indicating that the shear forces applied during the test need to be higher in order to effectively organize and align the polymer and extract macromolecules [26, 29].

Electrospun mats: PLA/extract incorporation

To evaluate the interaction between the COE and the polymer, as well as its influence on the morphology of the fibers produced via electrospinning, the mats were characterized using SEM and contact angle measurement, as shown in Fig. 7.
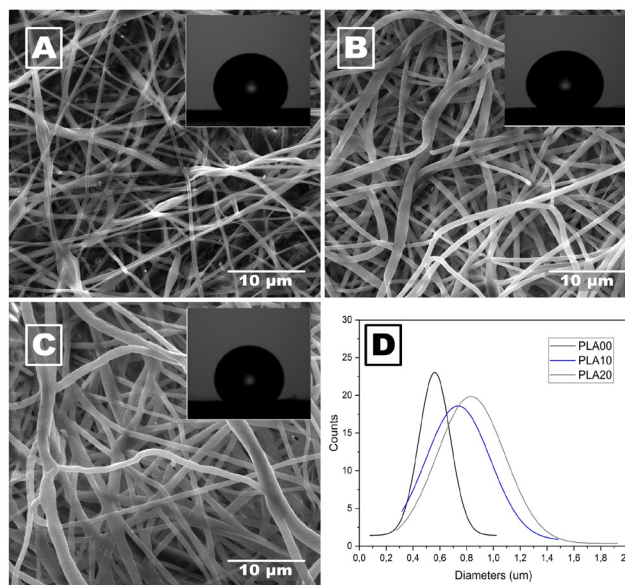

Figure 7. SEM images of the PLA mats with COE, as well as a histogram and a contact angle photograph: a) PLA00, b) PLA10, c) PLA20, d) comparative histograms for the PLA/COE samples
Source: Authors

Fig. 7a shows the morphology of the PLA00 fibers (602.6 ± 176.4 nm), which are uniform and free of defects. These were obtained under the processing conditions selected in the initial study. In contrast, the average fiber diameter obtained via electrospinning was lower than that reported for electrospun PLA fibers from a trifluoroethanol solution (16 wt. %, ~992 nm), demonstrating that the solvent system employed herein effectively reduces the diameter of the defect-free fibers [30].

As shown in Figs. 7b and 7c, it was possible to produce electrospun fibers incorporating COE at the two proposed concentrations (PLA10 and PLA20). A slight increase in fiber diameters was observed when adding 10 wt. % COE (787.9 ± 249.5 nm), which can be attributed to an increased solution viscosity (Fig. 5). In PLA20 (Fig. 7c), the fibers show a more heterogeneous diameter than those obtained with a higher extract concentration (963.2 ± 401.6 nm), as shown in Fig. 7d. The increase in the standard deviation on the fibers is primarily related to instability in the formation of the Taylor cone due to the high viscosity, indicating that this amount of extract requires higher voltages when compared to the other two solutions studied [31].

An interesting characteristic of the electrospun PLA mats with COE is that the incorporation of the extract did not

enhance the hydrophilicity of the mats, maintaining a contact angle of approximately 134° (Fig. 7). In contrast, [13] reported a reduced contact angle with a natural, unmodified extract. This difference can be attributed to the commercial multicomponent extract used in our study (Linitul), whose excipients modulate surface interactions and prevent significant variations in wettability [1].

Chemical evaluation of the PLA/extract mats

The chemical composition and interaction of the electrospun PLA mats, with and without extract, were evaluated using FTIR spectroscopy. The spectrograms of the samples PLA/ Coe are presented in Fig. 8.
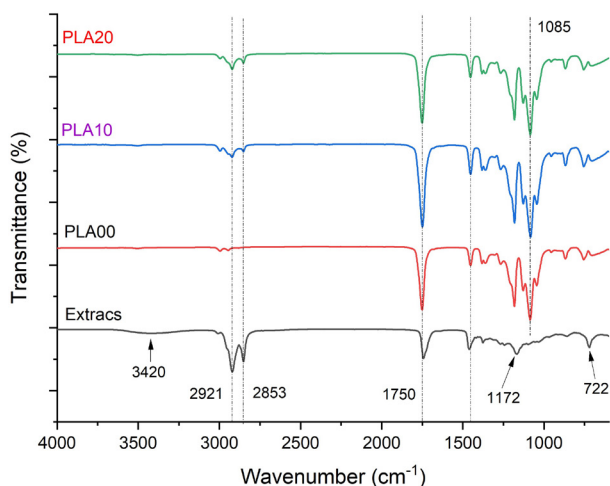

Figure 8. Comparative FTIR-ATR spectrogram of PLA mats with and without COE
Source: Authors

Fig. 8 compares the FTIR spectrums of the electrospun PLA mats, revealing key features that are indicative of the polymer's chemical structure. The mats (PLA00, PLA10, and PLA20) show a prominent peak at approximately 1750 cm^{-1}, which corresponds to the carbonyl (C=O) stretching vibration of the ester groups, typical of the lactide units in the PLA. The ester functionality is further confirmed by the 1195 cm^{-1} band, associated with C-O stretching vibrations. Additionally, the spectrum exhibits peaks around 1445 cm^{-1}, attributed to C-H bending vibrations, which are indicative of the methyl and methylene groups within the polymer chain. The C-O-C stretching vibration of the PLA backbone is observed in 1085 cm^{-1} [16], [19], [32].

As for the FTIR spectrogram of the active material (COE), characteristic bands are evident at 3400 and 2921 cm^{-1}, attributed to the overtone vibrations of the methyl group (-OH), which indicates the presence of castor oil at higher concentrations of the commercial cream. This is supported by the presence of characteristic bands, in addition to that observed in [33]. The flexural vibrations of aliphatic methylene and methyl C-H bonds at 1455 and 1380 cm^{-1} suggest the presence of a saturated hydrocarbon in the oil.

On the other hand, stretching vibrations (C=C), as well as bending CH vibrations of the benzene ring in the range of 910 to 723 cm^{-1}, suggest the presence of aromatic rings in the extract used [17], [34].

Thermal behavior of the electrospun mats

Fig. 9 shows a comparative thermogram for the COE and PLA mats with and without extract. The thermal stability of the mats studied in this work was evaluated using by means of TGA.
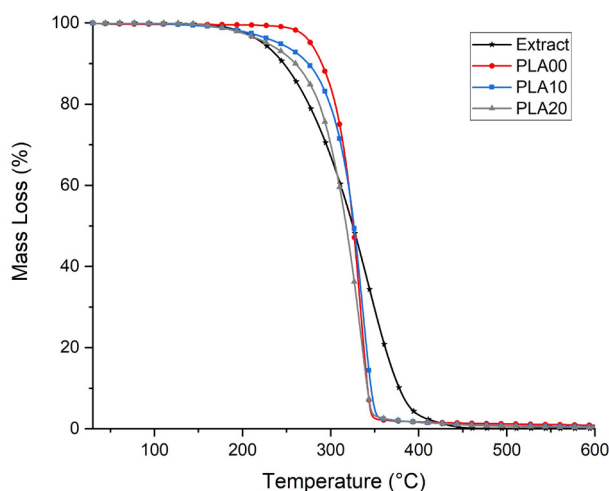

Figure 9. Comparative thermogram for the *Ricinus communis* extract and the PLA mats with and without COE
Source: Authors

This figure compares the thermal stability of the COE, PLA00, PLA10, and PLA20. All PLA-based samples exhibited a single mass-loss event associated with the thermal degradation of the polymer, occurring between approximately 290 and 370 °C—this is consistent with values reported in the literature [35]. The commercial COE, in contrast, degraded over a broader temperature range (150-460 °C), reflecting its complex composition. The incorporation of COE into PLA slightly reduced the onset degradation temperature (T_{onset}) by about 10-15 °C compared to the neat PLA fibers, suggesting that the presence of the low-molecular mass components in the COE promotes an earlier onset of thermal decomposition. However, the main degradation step remained within the typical range for PLA, indicating that the overall thermal stability was largely preserved. No mass loss was observed below 100 °C, confirming a complete solvent removal during the electrospinning process [36].

These results contrast with those reported by [13], who observed a significant increase in the onset degradation temperature (T_{onset}) for PLA blends with castor oil, given their use of a pure extract with higher thermal stability (T_{onset} of 344 °C) compared to neat PLA (T_{onset} of 264 °C). In this study, however, the commercial extract used showed a lower T_{onset} than the neat PLA, likely due to the presence of excipients or low-molecular-weight volatile compounds that

promote an earlier thermal degradation [37]. Despite this reduction in T_{onset}, the PLA/COE blends exhibited a higher overall thermal stability compared to neat PLA, a behavior observed in electrospun PLA/*M. officinalis* extract samples [38]. This behavior can be attributed to the plasticizing effect of the extract, which increases polymer chain mobility and allows for a more efficient distribution of thermal energy, thereby delaying the progression of degradation throughout the material.

The thermal transition of the electrospun PLA/COE mats was evaluated via DSC. The thermal stages are depicted in Fig. 10 and Table 1.
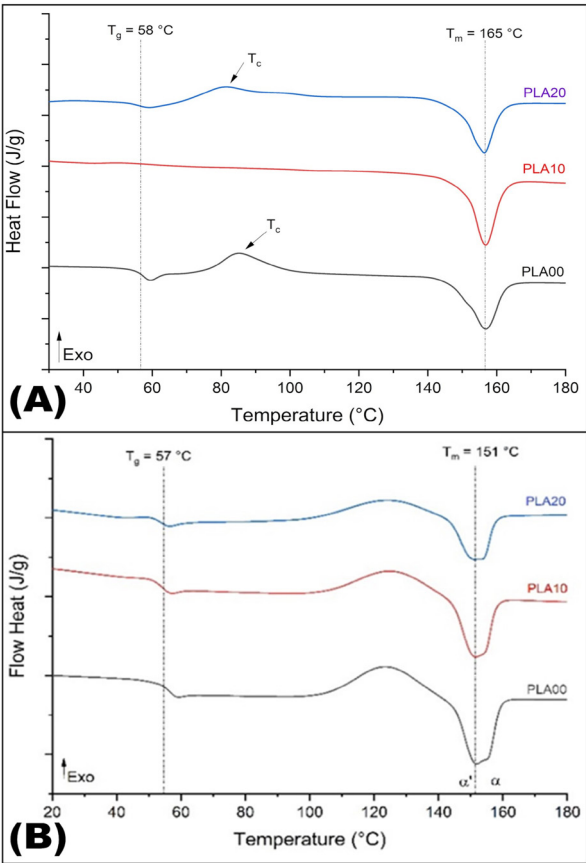

Figure 10. DSC thermogram of electrospun mats with varying COE concentrations: a) first heating cycle, b) second heating cycle
Source: Authors

Fig. 10a shows the first heating cycle of the electrospun PLA/COE mats, illustrating the thermal transitions associated with the electrospinning process. In PLA00 and PLA20, an exothermic crystallization peak is observed at 81 and 85°C, respectively, which is typical of amorphous PLA. However, this peak is absent in PLA10, suggesting that, at this concentration, the extract may promote a more complete crystallization.

As for the second heating cycle (Fig. 10B), all samples show a glass transition (Tg) near 55-58 °C. Although the PLA/COE samples exhibited slightly lower Tg values (by about 2 °C) compared to the neat PLA (PLA00). This variation falls within the expected experimental error of DSC measurements [40]. Therefore, it cannot be conclusively interpreted as a plasticizing effect based on Tg alone. However, this subtle shift, when considered together with other thermal indicators, such as the reduction in crystallinity (Table I) and fusion enthalpy, suggests a possible increase in chain mobility induced by the extract. This interpretation aligns with the known behavior of low-molecular-weight additives, which may act as plasticizer and disrupt the crystalline organization of PLA chains.

Furthermore, the melting temperature (Tm) profiles (Fig. 10b) display two endothermic peaks corresponding to distinct crystal populations (α′ and α). The incorporation of COE altered the relative intensity and enthalpy of these peaks, as shown in Table I, suggesting a reduction in the ordered crystalline domains. This supports the hypothesis that the extract interferes with the crystallization kinetics of PLA during electrospinning [15], [20].

These findings are in line with previous studies reporting the effect of natural additives on the thermal properties of PLA. For instance, [39] observed a reduction in the Tg and melting enthalpy of PLA upon incorporating *karanja* oil, indicating a plasticizing behavior and decreased crystallinity. [41] demonstrated that the addition of castor oil-derived plasticizers such as raw butyl ricinoleate (RBR) and castor oil glycidyl ether (COGE) lead to a substantial decrease in Tg (from 59.3 to 47.7 °C) and Tm, given the reduced intermolecular interactions and enhanced chain mobility. In contrast, [13] reported an increase in crystallinity and thermal stability when using pure castor oil, highlighting the role of extract purity and composition. The lower crystallinity and fusion enthalpy observed in our samples (PLA10 and PLA20)

Table I. Thermal stages in electrospun mats of neat PLA, and extracts variation in composition (PLA00, PLA10, and PLA20)

Sample	1st heat cycle					2nt heat cycle				
	TC [°C]	ΔHc [J/g]	Tm [°C]	ΔHm [J/g]	Xc [%]	Tg [°C]	Tc [°C]	Tm [°C]	ΔHm [J/g]	Xc [%]
PLA00	85,1	18,6	156,7	29,6	11,83	55,8	123,7	151,8	23,6	25,38
PLA10	--	--	156,8	25,2	27,10	53,7	124,6	151,6	13,1	14,09
PLA20	81,5	19,6	156,4	31,7	13,01	53,9	124,1	151,2	17,1	18,39

Source: Authors

suggest that Linitul interferes with the regular arrangement of PLA chains, which is likely due to the excipients used, supporting our interpretation of a plasticizing effect.

Mechanical behavior

The mechanical properties of the electrospun PLA mats with and without COE are shown in Fig. 11 and summarized in Table II. Fig. 11A presents the mechanical behavior of PLA00, PLA10, and PLA20.

All samples exhibited the typical behavior of ductile PLA mats, with deformation preceding failure. However, visible differences in stiffness and elongation were observed as a function of the COE content. The corresponding elasticity modulus, tensile strength, and elongation at break values are presented in Table II.
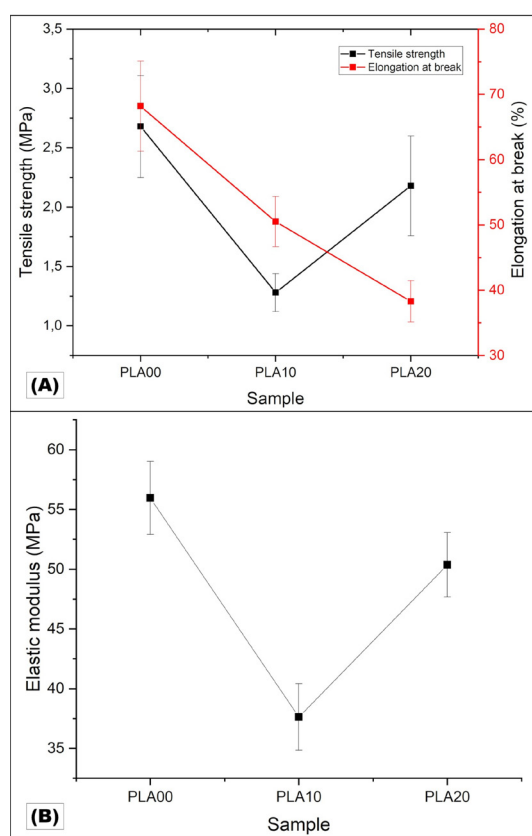

Figure 11. Mechanical behavior of electrospun PLA mats under varying COE concentrations: a) tensile strength and elongation at the break, b) elastic modulus
Source: Authors

Table II. Mechanical properties of PLA samples (mean ± stand and deviation)

Sample	Elastic modulus [MPa]	Ultimate tensile strength [MPa]	Elongation at break [%]
PLA00	55.72 ± 3.06	2.68 ± 0.43	68.2 ± 6.89
PLA10	37.63 ± 2.78	1.28 ± 0.16	50.5 ± 3.84
PLA20	50.37 ± 22.76	2.18 ± 0.42	38.3 ± 3.17

Source: Authors

Neat PLA (PLA00) showed the highest mechanical performance, with an elastic modulus of 55.72 ± 3.06 MPa, a tensile strength of 2.68 ± 0.43 MPa, and an elongation at break of 68.2 ± 6.89%. This is consistent with a stable amorphous structure without additives. Upon adding 10 wt.% COE (PLA10), all mechanical parameters decreased significantly: the modulus dropped to 37.63 ± 2.78 MPa, the tensile strength was halved (1.28 ± 0.16 MPa), and the elongation was reduced to 50.5 ± 3.84%. As for PLA20 (20 wt.% COE), the modulus partially recovered (50.37 ± 22.76 MPa), and the tensile strength increased to 2.18 ± 0.42 MPa, although the elongation continued to decrease (38.3 ± 3.17%). This trend suggests that COE initially acts as a plasticizer, reducing intermolecular interactions and flexibility, while higher concentrations may induce phase structuring or molecular re-entanglement, increasing stiffness at the cost of ductility.

These results can be directly compared to those of the study by [25], who evaluated electrospun mats using DMA. For pure polymer mats, a storage modulus of approximately 60 MPa at room temperature was reported, which aligns closely with our PLA00 (55.7 MPa), supporting the reproducibility of mechanical behavior in electrospun PLA-based systems. Upon blending with 20 wt.% PHBV, the authors observed a reduction in stiffness and a more flexible behavior, consistent with our PLA10. However, similar to our PLA20, their study also found that certain blend ratios partially recovered their mechanical strength, which can be attributed to changes in phase morphology and entanglement [25], [42].

Regarding miscibility, the mechanical results (Fig. 11b) are further supported by the viscosity data (Fig. 6b), which showed increasing viscosity with a higher COE content. This behavior contrasts with a pure plasticizing effect (which would decrease viscosity) and suggests a partial miscibility, with the possible formation of COE-rich domains or networked structures. This is in line with the interpretation proposed in literature, which links rheological behavior to component compatibility in polymer systems [43], [44].

Therefore, combining tensile, thermal (DSC), and rheological observations makes it evident that the PLA/COE system undergoes plasticization at low extract concentrations. However, it tends to form heterogeneous or semi-structured morphologies at higher concentrations, leading to a complex mechanical response that reflects both chain mobility and interfacial interactions.

Swelling capacity of the electrospun mats

The water absorption capacity of the electrospun PLA samples, with and without extracts, was evaluated by placing 1 x 1 cm samples of each film in a 0.1% sodium chloride (NaCl) saline solution for 24 h. The weight of the samples was measured at five different time points, as shown in Fig. 12.
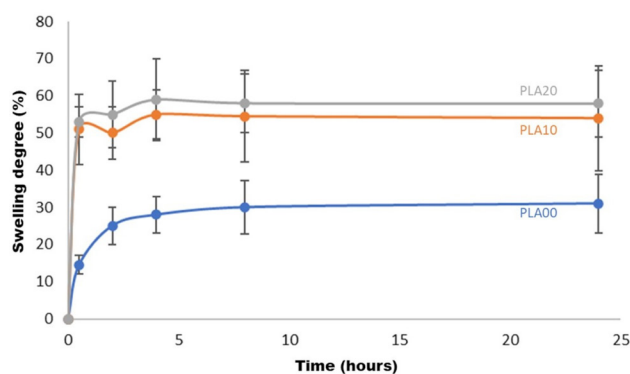
Figure 12. Swelling assay of PLA electrospun mats with and without COE using a physiological solution (0.1 wt.% NaCl)
Source: Authors

Fig. 12 shows that the incorporation of COE into PLA fibers significantly increased the swelling degree of the mats. After only 1 h, PLA10 and PLA20 reached swelling degrees of approximately 50 and 55%, respectively, remaining stable over 24 h. In contrast, the PLA00 mats exhibited a significantly lower and slower swelling response, stabilizing around 30%.

The swelling results observed in this study, particularly those for PLA10 and PLA20, which showed stabilized swelling degrees between 45 and 55%, are consistent with or superior to the values reported in the literature. For instance, [45] reported swelling capacities of up to 60% for PLA/PVA/SA-based electrospun membranes, while [46] reported values around 30-40% for PLA/chitosan systems. Similarly, [47] observed swelling levels between 20 and 40% for PLA loaded with curcumin. These comparisons highlight that the incorporation of COE not only imparts biofunctional activity but also enhances water uptake capacity, making the PLA/COE system particularly promising for applications in chronic wound dressings.

Thus, the observed increase in the swelling of PLA10 and PLA20 confirms that COE acts as a hydrophilic modifier. Despite the intrinsic hydrophobicity of PLA, the excipients present in the commercial extract appear to facilitate water penetration into the fiber network. This result reinforces the suitability of the PLA/COE system for wound healing applications, where maintaining a moist environment is critical for accelerated tissue repair [48], [49].

Conclusions

This study showcased the successful production of uniform, defect-free PLA fibers using a 15 wt.% solution, which yielded average diameters of 913.6 ± 99.1 nm. In contrast, fibers obtained from 20 wt.% PLA exhibited ribbon-like morphologies and defects due to jet instability and the loss of process control. The incorporation of 10-20 wt.% COE increased the fiber diameter and decreased the thermal stability (T_{onset} reduced by ~10-15 °C), which is consistent

with a plasticizing effect. The tensile analysis showed a drop in the elastic modulus, from 55.7 MPa (PLA00) to 37.6 MPa (PLA10), while the swelling capacity improved by up to 50%, indicating functional enhancements for wound management.

Partial miscibility between PLA and COE was suggested by increased viscosity and non-linear mechanical responses, highlighting complex phase interactions, likely influenced by excipients in the extract. This study did not address extract release or biological assays due to the intrinsic complexity of the commercial formulation. These limitations justify the current focus on structural and physicochemical compatibility. Future works will explore release kinetics, cytocompatibility, and degradation under physiological conditions to validate the system for biomedical applications such as chronic wound care.

Acknowledgements

Author contributions

J. M. Anaya-Mancipe: conceptualization, formal analysis, investigation, methodology, visualization, project administration, and writing (original draft). **J. A. Anaya-Mancipe**: formal analysis, investigation, methodology, visualization, writing (original draft). **M. N. da Conceição**: conceptualization, investigation, methodology, writing (original draft). **R. M. S. M. Thiré**: conceptualization, funding acquisition, methodology, supervision, writing (review and editing).

Conflicts of interest

The authors declare no conflict of interest regarding the publication of this paper.

References

[1]   A. C. Figueiredo, J. M. Anaya-Mancipe, A. O.S. Barros, R. Santos-Oliveira, M. L. Dias, and R. M. S. M. Thiré, "Nanostructured electrospun polycaprolactone-propolis mats composed of different morphologies for potential use in wound healing," *Molecules*, vol. 27, no. 16, art. 5351, 2022. https://doi.org/10.3390/molecules27165351

[2] J. M. A. Mancipe, F. A. Lobianco, M. L. Dias, and R. M. S. M. Thiré, "Electrospinning: New strategies for the treatment of skin melanoma," *Mini-rev. Medicin Chem.*, vol. 22, no. 4, pp. 564-578, 2022. https://doi.org/10.2174/i1389557521666210712111809

[3] M. L. L. Tan, J. S. Chin, L. Madden, and D. L. Becker, "Challenges faced in developing an ideal chronic wound model," *Expert Opin. Drug Discov.*, vol. 18, pp. 99-114, 2023. https://doi.org/10.1080/17460441.2023.2158809

[4] P. Mohite, A. Puri, D. Bharati, and S. Singh, "Polyphenols-encapsulation nanoparticles for the treatment of chronic metabolic diseases." In *Role of Flavonoids in Chronic Metabolic Diseases*, Hoboken, NJ, USA: John Wiley & Sons Ltd., 2024, ch. 11, pp. 375-416.

[5] B. Rajchal, Y. N. Thapa, D. Karki, P. Prajapati, and R. Adhikari, "Insights into electrospun polymeric nanofiber mats: an innovative dressing for wound healing applications," *Polym. Int.*, vol. 74, no. 5, pp. 391-404, 2024. https://doi.org/10.1002/pi.6736

[6] S. Zhu and L. Nie, "Progress in fabrication of one-dimensional catalytic materials by electrospinning technology," *J. Ind. Eng. Chem.*, vol. 93, pp. 28-56, 2021. https://doi.org/10.1016/j.jiec.2020.09.016

[7] J. M. A. Mancipe, S. G. Nista, G. E. R. Caballero, and L. H. I. Mei, "Thermochromic and/or photochromic properties of electrospun cellulose acetate microfibers for application as sensors in smart packing," *J. Appl. Polym. Sci.*, vol. 138, no. 11, art. 50039, 2021. https://doi.org/10.1002/app.50039

[8] G. L. G. Silva *et al.*, "Antibiotics-loaded nanofibers fabricated by electrospinning for the treatment of bone infections," *Arab. J. Chem.*, vol. 16, no. 1, art. 104392, 2023. https://doi.org/10.1016/j.arabjc.2022.104392

[9] P. Kumari, S. Sharma, P. K. Sharma, and A. Alam, "Treatment management of diabetic wounds utilizing herbalism: An overview," *Curr. Diabetes Rev.*, vol. 19, pp. 92-107, 2023. https://doi.org/10.2174/1573399981866622031809 5320

[10] V. R. Patel, G. G. Dumancas, L. C. K. Viswanath, R. Maples, and B. J. J. Subong, "Castor oil: Properties, uses, and optimization of processing parameters in commercial production," *Lipids Insights*, vol. 9, pp. 1-12, 2016. https://doi.org/10.4137/LPI.S40233

[11] E. C. Sanford, A. Muntz, and J. P. Craing, "Therapeutic potential of castor oil in managing blepharitis, meibomian gland dysfunction and dry eye," *Clin. Exp. Optom.*, vol. 104, no. 3, pp. 315-322, 2020. https://doi.org/10.1111/cxo.13148

[12] T. Tsujimoto, Y. Haza, Y. Yin, and H. Uyama. "Synthesis of branched poly(lactic acid) bearing a castor oil core and its plasticization effect on poly(lactic acid)," *Polym. J.*, vol. 43, pp. 425-430, 2011. https://doi.org/10.1038/pj.2011.3

[13] R. N. Darie-Niță *et al.*, "Evaluation of natural and modified castor oil incorporation on the melt processing and physico-chemical properties of polylactic acid," *Polymers*, vol. 14, no. 7, art. 3608, 2022. https://doi.org/10.3390/polym14173608

[14] S. K. Jaganathan, M. P. Mani, M. Ayyar, and E. Supriyanto, "Engineered electrospun polyurethane and castor oil nanocomposite scaffolds for cardiovascular applications," *J. Mater. Sci.*, vol. 52, pp. 10673-10685, 2017. https://doi.org/10.1007/s10853-017-1286-0

[15] D. M. Fernandes *et al.*, "Polymeric membranes base of on polylactic acid and babassu oil for wound healing," *Mater. Today Commnun.*, vol. 26, art. 102173, 2021. https://doi.org/10.1016/j.mtcomm.2021.102173

[16] J. F. Mendes *et al.*, "Obtaining poly(lactic acid) nanofibers encapsulated with peppermint essential oil as potential packaging via solution blow-spinning," *Int. J. Biol. Macromol.*, vol. 230, art. 123424, 2023. https://doi.org/10.1016/j.ijbiomac.2023.123424

[17] L. Dantas *et al.*, "Degradation kinetic of PLA compounds with castor oil," *J. Appl. Polym. Sci.*, vol. 141, no. 21, art. e55408, 2024. https://doi.org/10.1002/app.55408

[18]. F. Ciftci *et al.*, "Antibacterial and cellular behavior of PLA-based bacitracin and zataria multiflora nanofibers produced by electrospinning method," *Int. J. Polym. Mater. Polym. Biomater.*, vol. 72, no. 4, pp. 319-334, 2023. https://doi.org/10.1080/00914037.2021.2008391

[19] T. Jamnongkan *et al.*, "Innovate electrospun nanofibers mats based on polylactic acid composite with silver nanoparticles for medical application," *Polymers*, vol. 16, no. 3, art. 409, 2024. https://doi.org/10.3390/polym16030409

[20] J. M. Anaya-Mancipe *et al.*, "Electrospun nanofibers loaded with *Plantago major* L. extract for potential use in cutaneous healing," *Pharmaceutics*, vol. 15, art. 1047, 2023. https://10.3390/pharmaceutics15041047

[21] T. Saygili, H. T. Kahraman, G. Aydin, A. Avci, and E. Pehlivan, "Production of PLA-based AgNPs-containing nanofibers by electrospinning method and antibacterial application," *Polym. Bull.*, vol. 81, pp. 5455-5476, 2024. https://doi.org/10.1007/s00289-023-04956-6

[22] CIMA-AEMPS, "Linitul: Product information," Spain Agency of Medicines and Health Products, 2023. [Online]. Available: https://cima.aemps.es/cima/dochtml/p/32608/P_32608.html#6

[23] B. N. Teixeira, J. M. Anaya-Mancipe, and R. M. S. M. Thiré, "Evaluation of polycaprolactone nanofibers' using green solvent systems by solution blow spinning (SBS)," *Nanotechnology*, vol. 34, art. 5057017, 2023. https://doi.org/10.1088/1361-6528/acf8cd

[24] J. R. Sarasua, N. L. Rodríguez, A. L. Arraiza, and E. Meaurio, "Stereoselective crystallization and specific interactions in polylactides," *Macromolecules*, vol. 38, no. 20, pp. 8362-8371, 2005. https://doi.org/10.1021/ma051266z

[25]. A. Wagner, V. Poursorkhabi, A. Mohanty, and M. Misra, "Analysis of porous electrospun fibers from poly(L-lactic acid)/poly(3-hydroxibutyrate-co-3-hydroxyvalerate) blends," *ACS Sust. Chem. Eng.*, vol. 2, no. 8, pp. 1976-1982, 2014. https://doi.org/10.1021/sc5000495

[26] J. M. Anaya-Mancipe, A. C. de Figueiredo, L. G. Rabello, M. L. Dias, and R. M. S. M. Thiré, "Evaluation of the polycaprolactone hydrolytic degradation in acid solvent its influence on the electrospinning process," *J. Appl. Polym. Sci.*, vol. 141, no. 29, art. e55662, 2024. https://doi.org/10.1002/app.55662

[27] H. Karabulut, S. Unal, S. Ulag, A. Ficai, D. Ficai, and O. Gunduz, "Mapping the influence of solvent composition over the characteristics of polylactic acid nanofibers fabricated by electrospinning," *ChemistrySelect*, vol. 9, no. 17, art. e202301142, 2024. https://doi.org/10.1002/slct.202301142

[28] F. Topuz and T. Uyar, "Electrospinning of gelatin with tunable fiber morphology from round to flat/ribbon," *Mater. Sci. Eng. C*, vol. 80, pp. 371-378, 2017. https://doi.org/10.1016/j.msec.2017.06.001

[29] Y. Zhang *et al.*, "Preparation and numerical simulation of food gum electrospun nanofibers," *J. Food Eng.*, vol. 341, art. 111352, 2023. https://doi.org/10.1016/j.jfoodeng.2022.111352

[30] E. Y. Gómez-Pachón, R. Vera-Graziano, and R. M. Campos. "Structure of poly(lactic-acid) PLA nanofibers scaffolds prepared by electrospinning," *IOP Conf. Ser. Mater. Sci. Eng.*, vol. 50, art. 012003, 2013. https://doi.org/10.1088/1757-899X/59/1/012003

[31] R. P. O. Santos, L. A. Ramos, and E. Frollini, "Biobased electrospun mats composed of aligned and nonaligned fibers from cellulose nanocrystals, castor oil, and recycled PET," *Int. J. Biol. Macromol.*, vol. 163, pp. 878-887, 2020. https://doi.org/10.1016/j.ijbiomac.2020.07.064

[32] S. Visht, S. S. Salih, D. A. Mohammed, A. A. Abduljabbar, S. J. Hama, and I. A. Khudhair, "Formulation and evaluation of lip balm using different herbal pigment," *Pharmacogn. Res.*, vol. 16, no. 2, pp. 367-375, 2024. https://doi.org/10.5530/pres.16.2.46

[33] F. A. Atiku, A. A. Warra, and M. R. Enimola, "FTIR spectroscopic analysis and fuel properties of wild castor (*Ricinus communis* L) seed oil," *Open Sci. J. Anal. Chem.*, vol. 1, no. 1, pp. 6-9, 2014. "http://www.openscienceonline.com/journal/archive2?journalId=713&paperId=362"

[34] R. Zhang, Q. Shi, P. Hu, J. Ji, and Z. Suo, "Influence of castor oil-based bio-oil on the properties and microstructure of asphalt binder," *Constr. Build. Mater.*, vol. 408, art. 133564, 2023. https://doi.org/10.1016/j.conbuildmat.2023.133564

[35] D. H. S. Souza, P. V. Santoro, and M. L. Dias, "Isothermal crystallization kinetics of poly(lactic acid) stereo complex/graphene nanocomposites," *Mater. Res.*, vol. 21, art. e21070352, 2018. https://doi.org/10.1590/1980-5373-MR-2017-0352

[36] J. M. Anaya, M. L. Dias, and R. M. S. M. Thiré, "Avaliação morfológica de fibras eletrofiadas de policaprolactona em função do tipo de solvente," *Matéria (Rio J.)*, vol. 24, no. 3, art. e-12400, 2019. https://doi.org/10.1590/S1517-707620190003.0713

[37] E. M. Inácio, D. H. S. Souza, and M. L. Dias, "Thermal and crystallization behavior of PLA/PLLA-grafting cellulose nanocrystal," *Mater. Sci. Appl.*, vol. 11, pp. 44-57, 2020. https://doi.org/10.4236/msa.2020.111004

[38] N. Stoyanova *et al.*, "Electrospun PLA-based biomaterials loaded with *Melisa officinalis* extract with strong antioxidant activity," *Polymers*, vol. 15, no. 5, art. 1070, 2023. https://doi.org/10.3390/polym15051070

[39] N. I. Rahmat *et al.*, "Correlation study of glass transition temperature (T_g) of polymer blends using for equation and experimental values," *AIP Conf. Proc.*, vol. 3225, no. 1, art. 050001, 2025. https://doi.org/10.1063/5.0264721

[40] D. Garcia-Garcia, A. Carbonell-Verdu, M. P. Arrieta, J. López-Martínez, and M. D. Samper, "Improvent of PLA film ductility by plasticization with epoxidizer karanja oil," *Polym. Degrad. Stab.*, vol. 179, art. 109259, 2020. https://doi.org/10.1016/j.polymdegradstab.2020.109259

[41] Y. J. Yang and Q. Dou, "Plasticization of poly(lactic acid) by bio-based plasticizer derived from castor oil," *J. Polym. Environ.*, vol. 33, pp. 3241-3258, 2025. https://doi.org/10.1007/s10924-025-03612-6

[42] N. Kubiak *et al.*, "Sustainable PLA composites filled with poaceae fibers: Thermal, structural, and mechanical properties". *Materials*, vol. 18, no. 17, art. 3952, 2025. https://doi.org/10.3390/ma18173952

[43] J. M. Anaya-Mancipe *et al.*, "Solution blow spun with beaded-fiber morphologies as a drug delivery system with potential use for skin wound dressing," *ACS Appl. Mater. Interf.*, vol. 17, pp. 23466-23483, 2025. https://doi.org/10.1021/acsami.4c16675

[44] H. Qiao, A. Maazouz, and K. Lamnawar, "Study of morphology, and dynamic properties toward unveiling tha pertial miscibility in poly(lactic acid)-poly(hydroxybutyrate-co-hydroxyvalerate) blends," *Polymers*, vol. 14, no. 24, art. 5359, 2022. https://doi.org/10.3390/polym14245359

[45] H. Bi, T. Feng, and Y. Han, "*In vitro* and *in vivo* comparison study of electrospun PLA and PLA/PVA/SA fiber membranes for wound healing," *Polymer*, vol. 14, no. 4, art. 839, 2020. https://doi.org/10.3390/polym12040839

[46] J. Yin, L. Xu, and A. Ahmed. "Batch preparation and characterization of electrospun porous polylactic acid-based nanofiber membranes antibacterial wound dressing," *Adv. Fiber Mater.*, vol. 4, pp. 832-844, 2022. https://doi.org/10.1007/s42765-022-00141-y

[47] G. Perumal *et al.*, "Synthesis and characterization of curcumin loaded PLA-hyperbranched polyglycerol electrospun blend for wound dressing applications," *Mater. Sci. Eng. C*, vol. 76, pp. 1196-1204, 2017. https://doi.org/10.1016/j.msec.2017.03.200

[48] F. Pahlevanzadeh *et al.*, "Recent trend in three-dimensional bioinks based on alginate for biomedical applications," *Materials*, vol. 13, no. 18, art. 3980, 2020. https://doi.org/10.3390/ma13183980

[49] F. S. Pessanha *et al.*, "Effectiveness of epidermal growth factor loaded carboxymethylcellulose (EGF-CMC) hydrogel in biofilm in wound of diabetic patients: A randomized clinical trial," *Gel*, vol. 9, no. 2, art. 117, 2023. https://doi.org/10.3390/gels9020117